GSA DATA REPOSITORY 2011128 Melnik et al.

Supplementary material

1. CSD acquisition:

The groundmass plagioclase CSD (Fig. 1a and DR1d) was generated from element maps of 1024 by 800 points over an area of 1147 mm by 895 mm (pixels of 1.12 mm^2) of a carbon-coated polished thin section acquired by Energy Dispersive Spectrometry on a Hitachi S-3500N Scanning Electron Microscope at the University of Bristol. Aquisition details include an accelerating potential of 20 kV, working distance of 15 mm, count rate of 21,000 s^{-1} and dwell time of 50 ms. From element maps of Al, C, Ca, Fe, K, Mg, P, Si, Ti, the phase present at each point analysed was determined, and the relative proportion of each phase in the mapped area was calculated. For CSD calculations, the vesicle-free area was determined by subtracting the vesicle area (identified simply by high C) from the total area mapped. Plagioclase was identified by high Al and a limited range in Ca (DR1a,b). A binary bitmap for plagioclase was generated with all plagioclase pixels black and others white (DR1c). This phase map was filtered by replacing the centre value of an area of 3 by 3 pixels with the median value of all points within that area. The bitmap was inspected and crystals judged to be touching or obviously twinned were separated digitally by drawing a white line.

The 3D plagioclase CSD was determined with CSDCorrections version 1.3.9 (Higgins, 2000) from the apparent (2D) major axes of the ellipses determined with ImageJ software, and blocky crystals with relative axes dimensions of 1:1.4:2.9 determined with CSDSlice (e.g., Morgan and Jerram, 2006). Crystals touching the edge of the mapped area were not included in the analysis.

2. Supplementary Table DR1. Parameters used for the simulations:

Parameter	Notation	Value Unit		Ref.
Crystal density	ρ_c	2700	kg m^{-3}	S1
Melt density	ρ_m	2400	kg m^{-3}	S1
Discharge rate	Q	0.7	kg m^3/s	S2
Exit temperature	T_{atm}	980	C	S3
Initial melt water content	$c0$	6	wt%	S3
Solubility coefficient	C_f	4.1×10^{-6}	$Pa^{-1/2}$	S1
Latent heat of crystallization	Hc	3.02×10^5	J kg^{-1}	S1
Heat capacity	Cp	1200	J $kg^{-1}K^{-1}$	S1
Maximum growth rate	U_{max}	7.3×10^{-11}	m s^{-1}	S1
Maximum nucleation rate	J_{max}	10^{11}	m^{-3} s^{-1}	S1
Undercooling at U_{max}	ΔT_u	60	C	S1
Undercooling for J_{max}	ΔT_j	90	C	S1
Initial phenocryst content	β_{ch}	18	wt%	S4
Liquidus temperature	$T_m(p)$		C	S5
Crystallinity	$\beta(p,T)$		wt%	S5

3. Sensitivity analysis:

In order to test the sensitivity of the model to crystal growth kinetics parameterisation we have increased and decreased maximum nucleation rate by a half order of magnitude (Fig. 2). In the model growth rate and nucleation rate are linked by an assumption $n_{atm} = \frac{J\left(p_{atm}, T_{atm}, X_{atm}\right)}{U\left(p_{atm}, T_{atm}, X_{atm}\right)}$ where n_{atm} is obtained by extrapolation of measured CSD to L=0, p_{atm} and T_{atm} are the pressure and the temperature at the top of the conduit, and X_{atm} is the mass fraction of crystals at z=0 calculated from the CSD. As a basic set of parameters we use $J_{max}= 10^{11}$ $m^{-3}s^{-1}$ corresponding to $U_{max}= 7.3 \times 10^{-11}$ m s^{-1}. Short dashed curve corresponds to $J_{max}= 5 \times 10^{11}$ $m^{-3}s^{-1}$ ($U_{max}= 3.6 \times 10^{-10}$ m s^{-1}), long

dashed curve to J_{max}= 2x10^{10} m^{-3}s^{-1} (U_{max}= 1.5x10^{-11} m s^{-1}). These parameters are in the range of reported values for different andesitic volcanoes. Simulations show minor sensitivity for pressure (see Fig. DR2, inset), crystal content and temperature distributions inside the conduit. Also the transition to the chamber occurs at similar depth in all cases, demonstrating the power of the method to yield robust chamber depths. Sensitive parameters are, of course, nucleation and growth rate that scale according to their maximum values and the cross-sectional area of the conduit. However, when we multiply calculated cross-section areas by the ratio of maximum nucleation rates the results show good scaling and collapse to more or less uniform shapes. The biggest difference is between the cases of increased (x 5) and base (x 1) nucleation rates because in the upper part of the conduit the pressure distribution in these cases differs significantly. For higher nucleation rate (x 5) the calculated cross-section area of the conduit is smaller and conduit resistance plays an important role in the shallow part of the conduit.

Another uncertainty results from discharge rate determination. We made simulations for Q = 0.5, 0.7 (base value) and 0.9 m^{3}s^{-1}. The distribution of all parameters collapse to one curve if the cross-section area is normalized to a ratio of discharge rates (Fig. DR3).

Performed calculations suggest a natural normalizing factor for the cross-section area of the conduit as U_{max}*Q. As long as the pressure distribution remains close to hydrostatic (i.e. conduit resistance gives minor contribution to the pressure drop) distributions of all parameters will be very similar if cross-section of the conduit is normalized.

Supplementary References:

S1. O. Melnik, R.S.J. Sparks, Controls on conduit magma flow dynamics during lava dome building eruptions, J. Geophys. Res. 110 (B022) (2005), doi:10.1029/2004JB003183.

S2. Swanson, D.A., and Holcomb, R.T., 1990, Regularities in growth of the Mount St. Helens dacite dome, 1980–1986, *in* Fink, J.H., ed., Lava flows and domes, emplacement mechanisms and hazard implications: Berlin, Springer-Verlag, International Association of Volcanology and Chemistry of the Earth's Interior, Proceedings in Volcanology 2, p. 3–24.

S3. Blundy, J., Cashman, K., Berlo, K. Evolving magma storage conditions beneath Mount St. Helens inferred from chemical variations in melt inclusions from the 1980-1986 and current eruptions. chap. 33 of Sherrod, D.R., Scott, W.E., and Stauffer, P.H., eds., *A volcano rekindled; the renewed eruption of Mount St. Helens, 2004–2006*: U.S. Geological Survey Professional Paper **1750**, 755-790 (2008).

S4. Blundy, J., Cashman, K. Rapid decompression-driven crystallization recorded by melt inclusions from Mount St Helens volcano. *Geology* **33**, 793-796 (2005).

S5. Berlo, K., Blundy, J., Turner, S., Hawkesworth, C., 2007. Textural and chemical variation in plagioclase phenocrysts from the 1980 eruptions of Mount St. Helens, USA. *Contributions to Mineralogy and Petrology* **154**, 291-308.

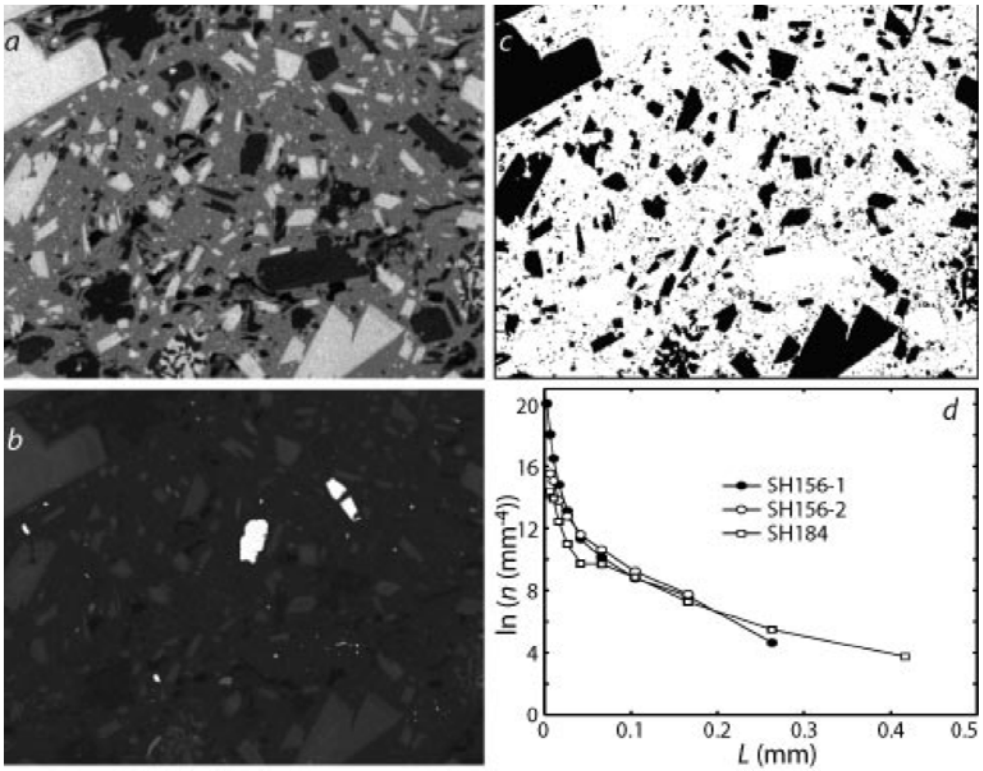

Figure DR1. (a) Al map (b) Ca map, c) plagioclase map for sample SH156-2, all 1230 mm by 960 mm. (c) is derived from (a) and (b) with black indicating plagioclase present (d) population number density versus crystal size (long axis of smallet ellipsoid fit) for sample SH156-2 as in Fig. 1a compared with equivilent data from two other samples erupted in 1984: SH156-1 also erupted 17 June and SH184, erupted 11 September. The groundmass of sample SH156-2 consists of 36% crystals (excluding vesicles) of plagioclase (75%), orthopyroxene (16%) and lesser amounts of Fe-Ti oxide, apatite and clinopyroxene.

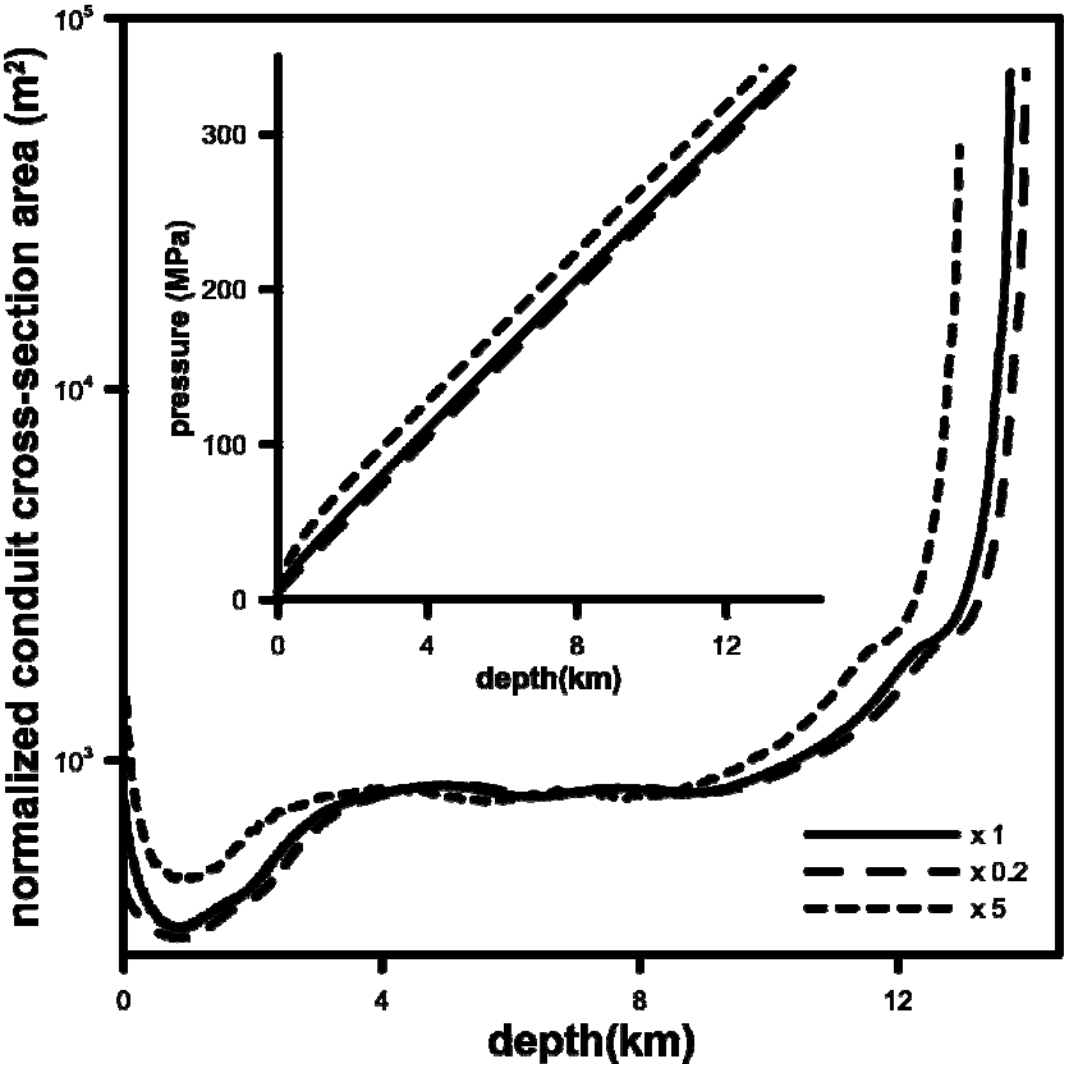

Figure DR2. Distributions of normalized cross-section and pressure (inset) with depth for three different maximum nucleation rates.

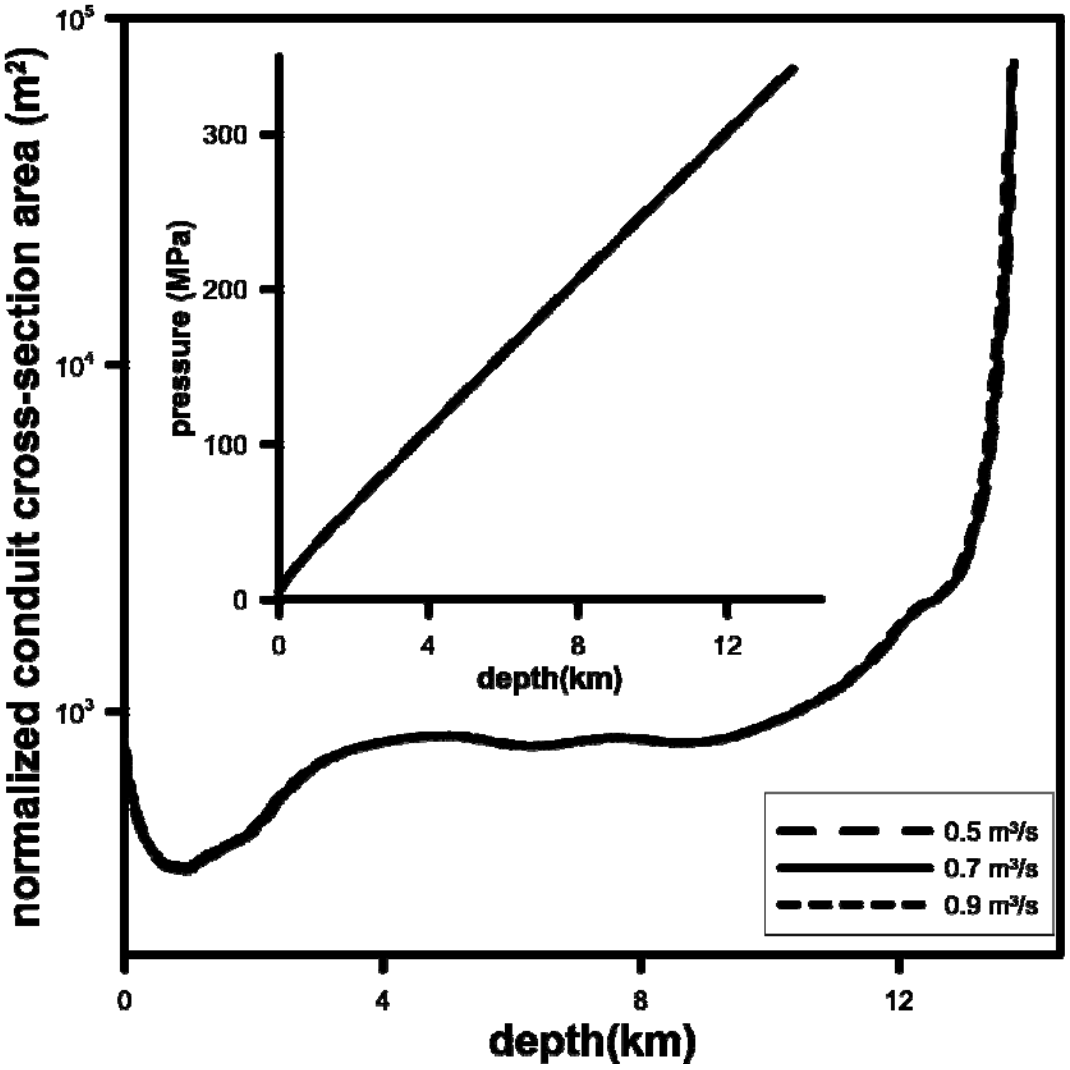

Figure DR3. Distributions of normalized cross-section and pressure (inset) with depth for three different discharge rates.